

Large-scale Vision-Language Models Learn Super Images for Efficient and High-Performance Partially Relevant Video Retrieval

Taichi Nishimura, Shota Nakada, Masayoshi Kondo
LY Corporation

Abstract

In this paper, we propose an efficient and high-performance method for partially relevant video retrieval (PRVR), which aims to retrieve untrimmed long videos that contain at least one relevant moment to the input text query. In terms of both efficiency and performance, the overlooked bottleneck of previous studies is the visual encoding of dense frames. This guides researchers to choose lightweight visual backbones, yielding sub-optimal retrieval performance due to their limited capabilities of learned visual representations. However, it is undesirable to simply replace them with high-performance large-scale vision-and-language models (VLMs) due to their low efficiency. To address these issues, instead of dense frames, we focus on super images, which are created by rearranging the video frames in a $N \times N$ grid layout. This reduces the number of visual encodings to $\frac{1}{N^2}$ and compensates for the low efficiency of large-scale VLMs, allowing us to adopt them as powerful encoders. Surprisingly, we discover that with a simple query-image attention trick, VLMs generalize well to super images effectively and demonstrate promising zero-shot performance against SOTA methods efficiently. In addition, we propose a fine-tuning approach by incorporating a few trainable modules into the VLM backbones. The experimental results demonstrate that our approaches efficiently achieve the best performance on ActivityNet Cap-tions and TVR.

1. Introduction

With the explosive increase of videos on the web, text-to-video retrieval (T2VR), a task of searching relevant videos to the input text query, has garnered significant attention in computer vision and natural language processing [6, 8, 16, 19, 27, 35, 40]. Current T2VR assumes that videos are pre-trimmed with short duration and that the input text queries are single sentences fully relevant to the videos. However, in practice, videos are generally untrimmed with long duration and contain multiple moments [4, 22, 45, 46]. For this reason, the input query typically pertains to specific

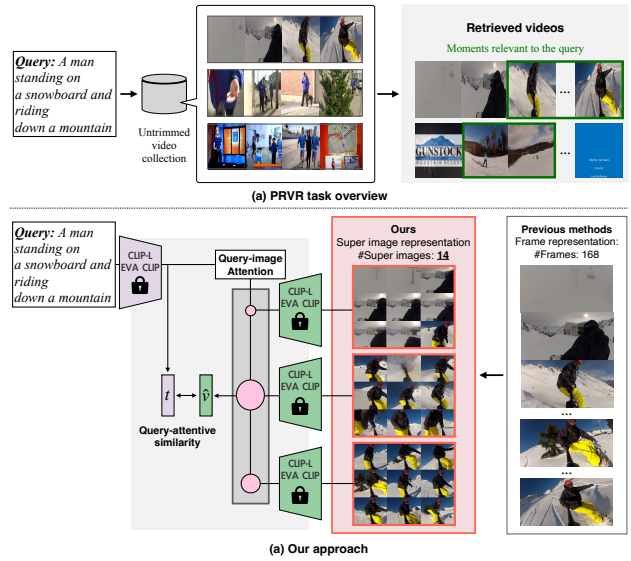


Figure 1. (a) Overview of the PRVR task. (b) The key concept of our approach. Super images are created by rearranging the frames in a $N \times N$ grid layout, enabling the model to reduce the number of visual encodings. With a simple query-image attention trick, large-scale VLMs generalize well to super images and show promising performance against the SOTA methods.

moments within the videos, rather than encompassing their entire content. To fit T2VR to the real-world scenario, partially relevant video retrieval (PRVR) was proposed [10], which aims at retrieving videos that contain at least one relevant moment with the query (Figure 1 (a)). For practical use for PRVR, it is essential to achieve high computational efficiency and retrieval performance. To address this goal, previous studies [10, 11] proposed a method to link a text query with the dense frame representations.

In terms of both efficiency and performance, the important but overlooked bottleneck of previous methods is the visual encoding of dense frames. From an efficiency perspective, dense frames require a model to encode the increased number of frames, leading to a rise in computation costs especially for long videos. To relieve them,

previous methods chose lightweight backbones such as ResNet152 [17] and CLIP-B/32 [33]. This backbone choice may yield performance issues due to its limited capabilities of learned visual representations compared with large-scale vision-and-language models (VLMs), such as CLIP-L/14 and EVA CLIP [14]. A recent study demonstrated that VLMs follow a scaling law [21], wherein increased model sizes correlate with enhanced performance on downstream tasks, thus larger VLMs are expected to improve the retrieval performance on PRVR. However, simply replacing the backbone with such VLMs is undesirable because they suffer from low efficiency, consuming much higher GFLOPs. For example, the EVA02-L-14 [14] visual backbone consumes 162.0 GFLOPs to encode a single image, which is considerably higher than the lightweight visual backbones of ResNet152 (=11.6 GFLOPs) and CLIP-B/32 (=8.8 GFLOPs). Therefore, a dilemma arises in balancing computational efficiency and high performance when leveraging large-scale VLMs, and one potential solution is to reduce the number of visual encodings. The most famous approach of such *less is more* ideas is sparse sampling [24, 25, 39], but is not suitable for PRVR because it requires a model to focus on local moments in the long videos, and sparse sampling miss them.

In this study, we overcome these difficulties and propose an efficient and high-performance PRVR method that employs large-scale VLMs (Figure 1 (b)). Instead of encoding dense frames or relying on sparse sampling, we focus on super images [12], which are created by rearranging the video frames in a $N \times N$ grid layout. This reduces the number of visual encodings to $\frac{1}{N^2}$ and compensates for the low efficiency of large-scale VLMs, allowing us to adopt them as a powerful image-text encoder. Then, two natural questions arise: (1) *how much do large-scale VLMs generalize well to super images for PRVR?* and if yes, (2) *how can we achieve an efficient and best-performance method by combining them and super images?* In terms of (1), although large-scale VLMs generalize to various kinds of images, such as natural images, computer screens, cartoons, and red circles in images [20, 34, 42], no previous research reported whether they can handle super images. In terms of (2), previous studies validated the high efficiency and good performance of using super images in uni-modal vision tasks, such as action recognition and deep fake detection [12, 39, 44], but it remains unclear whether the super images are effective for the cross-modal domain.

To answer these research questions, we investigate two scenarios for the PRVR task: zero-shot and fine-tuning settings. Surprisingly, with a simple query-image attention trick, large-scale VLMs can represent super images effectively and demonstrate promising zero-shot performance against SOTA methods that use lightweight visual backbones on public datasets, ActivityNet Captions [22] and

TVR [23]. Moreover, the fine-tuning approach enhances the capabilities of VLMs and achieves the best performance by introducing minimal trainable modules. The insights gained from varying the grid size, input image resolution, and backbone VLMs are two-fold: (1) the grid size and image resolution are trade-off parameters between retrieval performance and computation costs, and (2) the choice of VLMs significantly influences the overall performance.

2. Related work

2.1. Text-to-video retrieval

T2VR [6, 8, 9, 16, 19, 27, 35, 40] aims at searching relevant videos with the input text query from a collection of pre-trimmed videos with short duration. Traditional T2VR approaches encode videos and queries, convert them into joint embedding spaces, and compute the cross-modal similarity. Recently, as image-text VLMs [14, 33] have strong capabilities of zero-shot text-to-image retrieval performance, researchers have made tremendous efforts in training video-text VLMs [2, 24, 31, 43]. They reported that pre-trained video-text VLMs also achieved outstanding performance on the zero-shot T2VR tasks.

T2VR assumes that videos are pre-trimmed and the queries are fully relevant to them. However, in practice, videos are untrimmed with multiple moments [4, 22, 45, 46], and the queries are partially relevant to them. To fit the task for the practical scenario, PRVR was proposed [10], which aims at searching videos partially relevant to the input query. Previous studies tackled this task by employing fine-grained matching between the text queries and frame-level dense representations. Dong *et al.* [10] proposed multi-scale similarity learning (MS-SL), which constructs the multiple clips from the encoded frame-level representations as candidate moments and computes the cross-modal similarity between the clips and text queries. In [11], inspired by VLM capabilities, they proposed DL-DKD, where student branches learn the cross-modal similarity distribution between the frames and input query from the teacher branch of CLIP-B/32, a lightweight VLM backbone. Note that they also reported that training a model only with CLIP-B/32 features based on [3] does not reach the best performance because CLIP-B/32 fails to capture the matching between the query and untrimmed videos that contain mixed relevant and irrelevant moments to the query.

In previous studies, large-scale VLMs are not tested on PRVR because of their high computation costs to extract frame-level representations. This study addresses this problem by using super images to reduce the number of visual encodings and enable us to adopt large-scale VLMs.

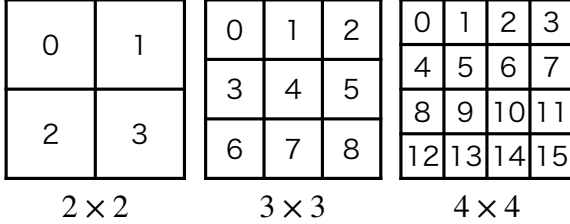


Figure 2. Examples of square grid layout used in [12]. This study uses 2×2 , 3×3 , and 4×4 square layouts in the experiments.

2.2. Summarized video representations

To mitigate computational costs, researchers have been pursuing effective video representations for downstream tasks. Summarized video representations [5, 7, 12, 32, 36, 37, 44] is one of the research directions that focuses on extracting compressed video features without compromising the essential information for downstream tasks. The mainstream is to represent videos as single images by summarizing RGB and motion in a video. Representative approaches include dynamic image network [5], informative frame synthesis [32], adaptive weighted spatio-temporal distillation [37], and adversarial video distillation [36].

Instead of representing videos as single images, super images for action recognition (SIFAR) [12] proposed super images created by rearranging video frames. They reported that pre-trained image encoders (e.g., Swin Transformer [29]) fine-tuned on super image representations can achieve higher performance with smaller GFLOPs than the SOTA methods. The idea of super images was exported into deep fake detection [44], yet not validated on cross-modal domains. This work is the first attempt to utilize super images for PRVR, demonstrating the effectiveness of super images on the cross-modal domains.

3. Approach

In this section, we describe our zero-shot and fine-tuning approaches. We first introduce background on super images in Section 3.1 and then describe the zero-shot and fine-tuning approaches in Section 3.2 and 3.3. We emphasize that the novelty of our work is to combine large VLMs and super images for efficient and high-performance PRVR, and the network architecture itself is not novel. In Section 4.2.1 and 4.2.2, we discover that zero-shot approaches efficiently achieve promising performance against the SOTA methods trained on each dataset and fine-tuned versions significantly outperform them.

3.1. Preliminary: super images

Super images were first proposed in [12] for action recognition. Given sequential video frames, they are ordered by

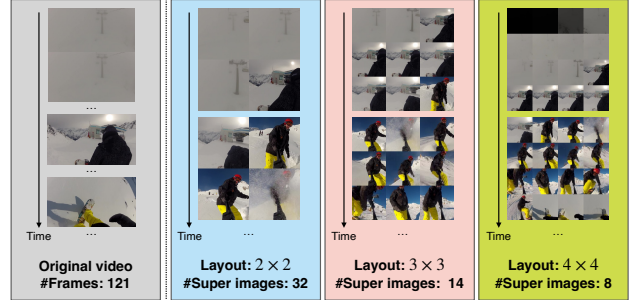


Figure 3. A Comparison of the original video frames and the created super images in different layouts: 2×2 , 3×3 , and 4×4 .

a pre-defined layout to form a super image. Figure 2 shows a square grid layout that SIFAR used. They reported that among various layouts, the square layout achieved the best performance across different datasets because it may encourage the models to learn temporal relationships between frames. As with SIFAR, this work uses the same layout.

To create super images, SIFAR first chooses the number of sampling frames M , samples frames uniformly, and forms a super image by placing them in order onto a grid of size $(N - 1) \times N$ when $M < (N - 1) \times N$ or $N \times N$ when $M \geq (N - 1) \times N$ where $N = \lceil \sqrt{M} \rceil$. Empty images are padded at the end if the grid is not full. Based on this idea, for example, 8 frames and 16 frames are fit into 3×3 and 4×4 layouts, respectively.

SIFAR sparsely samples frames by choosing M beforehand and creates single super images that capture the global content of videos. However, it is not suitable for our task because PRVR requires models to capture local moments in the videos, and single super images via sparse sampling likely miss them. We thus set frame per second (FPS), sample frames, and create sequential super images by fitting them into the pre-defined grid layout. Figure 3 shows a comparison of the original video frames and created sequential super images. We can observe that when increasing a grid size N , the number of super images decreases quadratically, and objects in each grid become smaller. In Section 4.2.1, we delve into this matter, exploring the optimal grid size that enables models to achieve high performance efficiently.

3.2. Zero-shot approach

In this setting, we tackle the task of retrieving super images from the corresponding partially relevant query without fine-tuning each dataset. Let (\mathbf{V}, \mathbf{t}) be positive pairs in the test set \mathcal{D}_{test} , where $\mathbf{V} = (v^1, v^2, \dots, v^k, \dots, v^K)$ and \mathbf{t} represents super images and text query, respectively (K is the number of super images). Given \mathbf{t} , our task is to retrieve corresponding \mathbf{V} from a collection of videos, yet partial images correspond to the query on PRVR, rather than

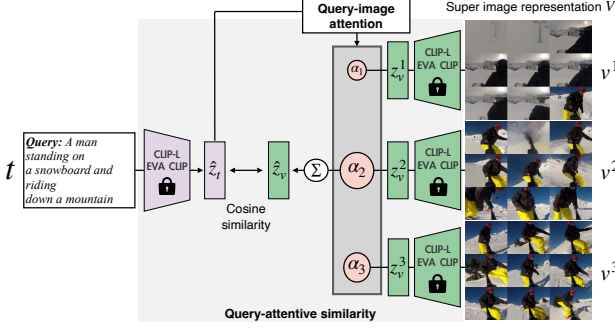


Figure 4. Overview of the zero-shot QASIR, which first encodes super images and a text query into vectors $(\mathbf{Z}_v, \mathbf{z}_t)$, computes a query-attentive visual vector $\hat{\mathbf{z}}_v$, and finally calculates the cosine similarity $\cos(\hat{\mathbf{z}}_v, \hat{\mathbf{z}}_t)$ as a similarity score.

matching the whole content of \mathbf{V} and \mathbf{t} . Therefore, globally aggregating \mathbf{V} does not perform well.

To address this problem, this study proposes a simple yet effective trick, namely query-attentive super image retrieval (QASIR), which aggregates \mathbf{V} by attending \mathbf{t} to compute similarity with an attention mechanism [1] (Figure 4). Specifically, the vision and text branches of VLMs convert super images \mathbf{V} and a query \mathbf{t} into their latent representations $\mathbf{Z}_v \in \mathbb{R}^{K \times d}$ and $\mathbf{z}_t \in \mathbb{R}^d$ as:

$$\mathbf{Z}_v = (z_v^1, z_v^2, \dots, z_v^k, \dots, z_v^K), \quad (1)$$

$$z_v^k = \text{VLM}_v(v^k), \quad (2)$$

$$z_t = \text{VLM}_t(\mathbf{t}), \quad (3)$$

where $\text{VLM}_v(\cdot)$, $\text{VLM}_t(\cdot)$ are the vision and text branches of VLMs and d represents the dimension of the latent vectors. Then, the super image representations are aggregated into the query-attentive visual vectors $\hat{\mathbf{z}}_v$ as follows:

$$\alpha_k = \frac{\exp(z_v^k \cdot z_t)}{\sum_i \exp(z_v^i \cdot z_t)}, \quad (4)$$

$$\hat{\mathbf{z}}_v = \sum_k \alpha_k z_v^k. \quad (5)$$

The similarity scores are computed by cosine similarity between $\hat{\mathbf{z}}_v$ and \mathbf{z}_t . Note that no additional training parameters are introduced in this approach.

3.3. Fine-tuning approach

Based on the QASIR, we propose a fine-tuning method to boost its retrieval performance without harming the computational efficiency (Figure 5). We add two modules to QASIR: feature adapters and temporal encoder.

The feature adapters are based on CLIP adapter [15], which freezes the original VLM networks and trains additional small networks, e.g., multi-layered (typically two or three) perceptrons (MLPs) with activation functions. The

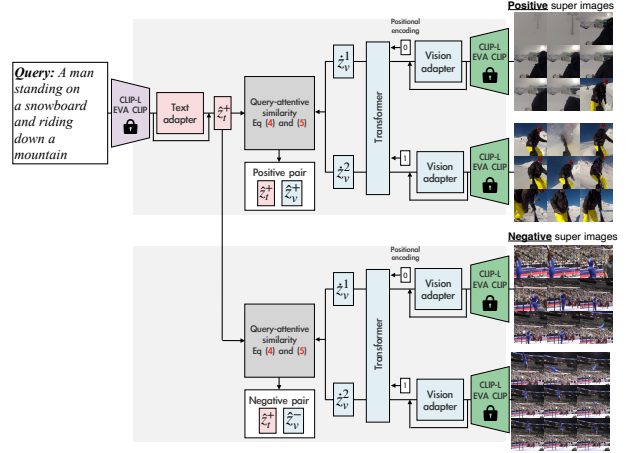


Figure 5. Overview of how to fine-tune QASIR. Given the textual query $\hat{\mathbf{z}}_t$, the model computes $\hat{\mathbf{z}}_t$ -weighted super image vectors for the positive $\hat{\mathbf{z}}_v^+$ and negative $\hat{\mathbf{z}}_v^-$ pairs. Then, their cosine similarity $\cos(\hat{\mathbf{z}}_v^+, \hat{\mathbf{z}}_t)$ and $\cos(\hat{\mathbf{z}}_v^-, \hat{\mathbf{z}}_t)$ is used for loss calculation.

researchers reported that compared with training all of the layers in VLMs, adaptation-based methods can achieve promising performance with minimum training costs, preventing the VLMs from catastrophic forgetting [18].

For simplicity, we focus on describing the vision branch. Instead of utilizing the output vector z_v^k from VLMs, the vision adapter computes \tilde{z}_v^k by interpolating z_v^k and the output vectors from MLPs as:

$$\tilde{z}_v^k = \beta_v z_v^k + (1 - \beta_v) \text{MLP}_v(z_v^k), \quad (6)$$

where $\text{MLP}_v(\cdot)$ represents the three layer MLPs with ReLU functions and β_v is a hyper parameter. Similarly, we prepare the text branch, dubbed text adapter, which acquires $\tilde{z}_t = \beta_t z_t + (1 - \beta_t) \text{MLP}_t(z_t)$, where $\text{MLP}_t(\cdot)$ is another MLPs that is same network structure to $\text{MLP}_v(\cdot)$. The architecture of MLPs is written in the supplementary materials.

The temporal encoder is introduced to represent the temporal information of super images. Modeling the temporal dependency is essential for video understanding tasks [41], thus we add a single-layer Transformer [38] into the vision side. Based on the super image vectors \tilde{z}_v^k from the vision CLIP adapter, we add positional encoding (PE) and input them into the Transformer as:

$$\hat{\mathbf{z}}_v^k = \text{Transformer}(\tilde{z}_v^k + \text{PE}(k)), \quad (7)$$

where $\text{Transformer}(\cdot)$ and $\text{PE}(\cdot)$ represents the Transformer layer and PE. Then, we acquire the query-attentive visual vectors $\hat{\mathbf{z}}_v^k$ by replacing z_v^k with $\hat{\mathbf{z}}_v^k$ in Eq (4) and Eq (5). The similarity scores are computed between $\hat{\mathbf{z}}_v^k$ and \tilde{z}_t .

Loss calculation. To fine-tune the model, as with CLIP [33], we use a symmetric cross-entropy loss over the simi-

larity scores. From an anchor query vector \hat{z}_t^+ , let the positive and negative super image vectors be \hat{z}_v^+, \hat{z}_v^- . Conversely, from an anchor super image vector \hat{z}_v^+ , let the positive and negative query vectors be \hat{z}_t^+, \hat{z}_t^- . The total loss of \mathcal{L} is computed as follows:

$$\mathcal{L} = \mathcal{L}_q + \mathcal{L}_i,$$

$$\mathcal{L}_q = \frac{1}{|\mathcal{B}|} \sum_{(z_v^+, z_t^+) \in \mathcal{B}} \log \left\{ \frac{\cos(z_v^+, z_t^+)}{\cos(z_v^+, z_t^+) + \sum_{z_v^- \in \mathcal{N}} \cos(z_v^-, z_t^+)} \right\},$$

$$\mathcal{L}_i = \frac{1}{|\mathcal{B}|} \sum_{(z_v^+, z_t^+) \in \mathcal{B}} \log \left\{ \frac{\cos(z_v^+, z_t^+)}{\cos(z_v^+, z_t^+) + \sum_{z_t^- \in \mathcal{N}} \cos(z_v^+, z_t^-)} \right\},$$

where $\mathcal{L}_q, \mathcal{L}_i$ represents query-to-image/image-to-query losses and \mathcal{B}, \mathcal{N} indicates the samples from mini-batch and negatives, respectively.

4. Experiments

4.1. Experimental settings

4.1.1 Datasets

We evaluate our methods on two PRVR datasets:

- **ActivityNet Captions** [22] collected YouTube videos and annotated them with event and sentence pairs. The average length of videos is 117.6 seconds, which is longer than TVR (=76.2 seconds). Following [10, 11], 10,009 videos with 37,421 events are used for training and 4,917 videos with 17,505 events are used for testing.
- **TV show Retrieval (TVR)** [23] is a multimodal dataset, containing 21.8K TV show videos with five sentences that describe a specific event in the video. As with [10, 11], 17,435 videos with 87,175 events are used for training and 2,179 videos with 10,895 events are used for testing.

4.1.2 Evaluation metrics

Performance metrics. As with previous PRVR studies [10, 11], we use Recall@ K ($K = 1, 5, 10, 100$), which computes the percentage of queries that correctly retrieve positive videos in the top K of the ranking list. We also report the sum of all recalls (sumR) for overall comparison.

Computation cost metrics. To evaluate the computational costs of the models, we report the total number of parameters (#parameters) for memory consumption and video-text GFLOPs for throughput, which computes the total number of floating point operations from visual/textual backbone encodings to video-text similarity calculation. The accurate definition of video-text GFLOPs is written in the supplementary material.

4.1.3 Comparative components

SOTA models with lightweight visual backbones. We compare our approaches with two SOTA methods that re-

ported the best scores on the PRVR task: MS-SL [10] and DL-DKD [11]. They use the same pre-extracted features on both visual and textual sides. On the visual side, I3D features extracted at 1 FPS and concatenated features of I3D and ResNet152 at 15 FPS are utilized for ActivityNet Captions and TVR, respectively. For the textual side, they use RoBERTa [28] for query feature extraction for both datasets. For TVR, RoBERTa was additionally fine-tuned on the queries and subtitle sentences of TVR. Note that DL-DKD uses CLIP-B/32, a relatively lightweight VLM backbone only for the training phase to transfer CLIP’s knowledge into the visual/textual features. They reported that using only CLIP-B/32 features does not perform well on PRVR and a hybrid approach of CLIP and CNN-based features can achieve the best retrieval performance.

Grid sizes, image resolution, and VLM backbones. To investigate how the grid sizes, image resolution, and VLM backbones affect the performance on PRVR, we prepare for four zero-shot and two fine-tuned models listed in Table 1. A comparison of different large-scale VLMs (OpenAI CLIP and EVA-02-CLIP) tests whether the choice of VLM affects the PRVR performance. In addition, a comparison of the input resolution of 224/336 and grid sizes of $1 \times 1, 2 \times 2, 3 \times 3$, and 4×4 tests whether the visibility of objects in super images affects the performance. Note that 1×1 is equivalent to the frame-level representations and means not using super images.

4.1.4 Implementation details

We set 0.5 FPS for the ActivityNet Captions and 3 FPS for TVR to obtain frames from the videos. Note that frames extracted at 3 FPS are officially distributed by the TVR authors, but raw videos are not due to copyright issues. For both vision and text adapters, we set the $\beta_v = \beta_t = 0.2$ as with [15] and hidden size to be 192. We fine-tune the model using the AdamW optimizer [30] with an initial learning rate of 0.0001. We set the batch size to 64, continue training at most 50 epochs, and use the weights that achieve the best performance on sumR.

4.2. Results

4.2.1 Zero-shot evaluation

Do large-scale VLMs generalize well to super images? Table 2 shows the zero-shot performance on the benchmark datasets. Surprisingly, the zero-shot QASIR with super images achieves promising performance against SOTA methods, which adopt lightweight visual backbones. In addition, half 2×2 models achieves comparable performance to 1×1 (± 3.0 sumR). These results indicate that large-scale VLMs can generalize to super images.

Balance between the retrieval performance and computation costs. QASIR is an efficient approach because its to-

	Model name	Resolution	Vision backbone	Text backbone	Parameters (M)
SOTA	MS-SL	224	I3D (+ResNet152)	RoBERTa [†]	433.3
	DL-DKD	224	I3D (+ResNet152, OpenAI CLIP-B/32*)	RoBERTa [†] (+OpenAI CLIP-B/32*)	439.0
Zero-shot	QASIR-L14	224		OpenAI CLIP-L/14	427.6 (-5.7)
	EVA-QASIR-L14	224		EVA-02-CLIP-L/14	427.8 (-11.2)
	QASIR-L14-336	336		OpenAI CLIP-L/14-336	427.9 (-11.1)
	EVA-QASIR-L14-336	336		EVA-02-CLIP-L/14-336	428.1 (-10.9)
Fine-tuned	QASIR-L14	224		OpenAI CLIP-L/14	431.0 (-8.0)
	QASIR-L14-336	336		OpenAI CLIP-L/14-336	431.3 (-7.7)

Table 1. A comparison of models. Note that when training the SOTA models on TVR, they utilize RoBERTa[†] fine-tuned on the queries and subtitle sentences of TVR. ResNet152 was additionally used only for TVR, not for ActivityNet Captions. DL-DKD uses CLIP-B/32* to transfer vision-and-language knowledge into visual and textual backbone in the training phase. **Red** values represent the decreased number of parameters (M) from DL-DKD.

	ActivityNet Captions							TVR						
	#Frames	GFLOPs	R@1	R@5	R@10	R@100	sumR	#Frames	GFLOPs	R@1	R@5	R@10	R@100	sumR
MS-SL [10]	118.2	3.4×10^3	7.1	22.5	34.7	75.8	140.1	5677.2	7.3×10^4	13.5	32.1	43.4	83.4	172.4
DL-DKD [11]	118.2	3.4×10^3	8.0	25.0	37.5	77.1	147.6	5677.2	7.3×10^4	14.4	34.9	45.8	84.9	179.9
QASIR-L14														
1×1	60.3	9.8×10^3	14.2	31.7	42.7	77.0	165.6	229.4	3.7×10^4	16.4	32.5	40.7	74.0	163.6
2×2	15.5	2.5×10^3	13.7	31.3	41.9	77.1	164.0	57.7	9.2×10^3	14.1	29.6	37.4	72.5	154.0
3×3	7.1	1.1×10^3	12.4	29.4	39.5	75.0	156.4	23.9	4.1×10^3	11.8	25.4	33.2	68.9	139.3
4×4	4.2	7.0×10^2	10.7	26.0	36.1	70.8	143.8	14.8	2.3×10^3	8.4	19.0	26.3	61.6	115.4
EVA-QASIR-L14														
1×1	60.3	9.8×10^3	17.3	36.6	48.0	79.2	181.0	229.4	3.7×10^4	11.3	23.8	30.9	64.7	130.7
2×2	15.5	2.5×10^3	16.8	36.1	47.4	79.8	180.1	57.7	9.2×10^3	9.2	20.5	27.1	61.6	118.4
3×3	7.1	1.1×10^3	15.0	33.8	44.9	77.9	171.7	23.9	4.1×10^3	8.3	18.2	24.8	59.4	110.7
4×4	4.2	7.0×10^2	12.4	29.4	39.7	73.6	155.1	14.8	2.3×10^3	5.3	13.4	18.8	51.2	88.8
QASIR-L14-336														
1×1	60.3	2.3×10^4	14.6	32.8	43.8	77.9	169.1	229.4	8.7×10^4	16.8	34.1	42.5	75.4	168.8
2×2	15.5	5.9×10^3	15.7	33.9	45.3	78.7	173.6	57.7	2.1×10^4	17.2	33.3	42.1	76.1	168.7
3×3	7.1	2.7×10^3	14.8	32.3	44.0	77.5	169.6	23.9	9.8×10^3	15.2	30.9	39.3	73.7	159.1
4×4	4.2	1.6×10^3	13.2	30.8	41.3	75.4	160.6	14.8	5.6×10^3	12.4	26.6	34.5	69.9	143.4
EVA-QASIR-L14-336														
1×1	60.3	2.3×10^4	18.6	38.3	49.2	80.7	186.8	229.4	8.7×10^4	13.8	27.0	35.3	68.1	144.3
2×2	15.5	5.9×10^3	19.0	38.9	50.2	81.4	189.6	57.7	2.1×10^4	12.8	25.7	33.1	67.4	138.9
3×3	7.1	2.7×10^3	17.5	36.7	48.4	80.0	182.6	23.9	9.8×10^3	11.1	23.2	30.5	65.3	130.0
4×4	4.2	1.6×10^3	15.3	33.8	45.1	77.9	172.1	14.8	5.6×10^3	8.9	19.5	26.5	61.5	116.4

Table 2. Zero-shot performance on the ActivityNet Captions and TVR dataset. **Bold** values represent the highest scores among each VLM and underlined values in video-text GFLOPs indicate that they are smaller than the SOTA methods.

tal #parameters are smaller than SOTA methods and some models with increased grid sizes achieve better performance and smaller video-text GFLOPs than them. It is worth noting that 2×2 with large-scale VLMs can reduce the computation costs to $\frac{1}{4}$ from 1×1 while minimizing the retrieval performance decrease. Therefore, combining super images and large-scale VLMs strikes a commendable balance between enhanced performance and computational costs.

Performance difference across datasets. QASIR consistently achieves higher performance than the SOTA methods on ActivityNet Captions but falls short in TVR. We notice that most nouns in queries are general objects (e.g., “man” and “dog”) in ActivityNet Captions while they are character names (e.g., “Sheldon”) in TVR. Although the training data for OpenAI CLIP is private and we cannot confirm this, one possible reason for the gap is that VLMs do not know these TV show characters and fail to link the character names and their visual representations.

Performance change when varying the grid size, input resolution, and VLM backbones. When changing the grid size, input resolution, and backbone VLMs, two insights emerge. First, the grid size and input resolution are key trade-off parameters between the performance and computation costs. As the input resolution increases and the grid size decreases, objects in each super image are more visible, yielding improved retrieval performance. However, this requires increased computation costs. Thus, it is essential to carefully select the optimal grid size and input resolution based on use cases. Second, the choice of VLMs has a substantial impact on overall performance. When comparing QASIR-L14-336 and EVA-QASIR-L14-336, the EVA-based model outperforms the CLIP-based one in ActivityNet captions; it falls short in TVR. EVA CLIP averagely performs better than OpenAI CLIP on image downstream tasks but is not consistently better in all of the tasks [13]. A careful selection of VLMs is important depending on the

Fully-trained	ActivityNet Captions						TVR					
	GFLOPs	R@1	R@5	R@10	R@100	sumR	GFLOPs	R@1	R@5	R@10	R@100	sumR
MS-SL [10]	3.4×10^3	7.1	22.5	34.7	75.8	140.1	7.3×10^4	13.5	32.1	43.4	83.4	172.4
DL-DKD [11]	3.4×10^3	8.0	25.0	37.5	77.1	147.6	7.3×10^4	14.4	34.9	45.8	84.9	179.9
QASIR-L14												
1 × 1	9.8×10^3	18.9 (+10.9)	41.0 (+16.0)	53.2 (+15.7)	84.8 (+7.7)	197.9 (+50.3)	3.7×10^4	23.6 (+9.2)	47.0 (+12.1)	56.5 (+10.7)	89.0 (+4.1)	216.1 (+36.2)
2 × 2	2.5×10^3	18.2 (+10.2)	39.6 (+14.6)	52.2 (+14.7)	84.8 (+7.7)	194.9 (+47.3)	9.2×10^3	23.0 (+8.6)	45.4 (+10.5)	56.3 (+10.5)	88.9 (+4.0)	213.6 (+33.7)
3 × 3	1.1×10^3	16.5 (+8.5)	37.5 (+12.5)	49.9 (+12.4)	83.2 (+6.1)	187.1 (+39.5)	4.1×10^3	21.0 (+6.6)	42.5 (+7.6)	54.0 (+8.2)	88.4 (+3.5)	205.8 (+25.9)
4 × 4	7.0×10^2	14.1 (+6.1)	33.8 (+8.8)	45.6 (+8.1)	80.4 (+3.3)	174.0 (+26.4)	2.3×10^3	16.3 (+1.9)	35.7 (+0.8)	46.4 (+0.6)	84.6 (+0.3)	182.9 (+3.0)
QASIR-L14-336												
1 × 1	2.3×10^4	19.7 (+11.7)	41.4 (+16.4)	53.9 (+16.4)	85.1 (+8.0)	200.1 (+52.5)	8.7×10^4	26.9 (+12.5)	50.6 (+15.7)	60.7 (+14.9)	91.4 (+6.5)	229.6 (+49.7)
2 × 2	5.9×10^3	19.3 (+11.3)	41.5 (+16.5)	53.8 (+16.3)	85.3 (+8.2)	200.0 (+52.4)	2.1×10^4	26.7 (+12.3)	50.6 (+15.7)	61.4 (+15.6)	91.4 (+6.5)	230.1 (+50.2)
3 × 3	2.7×10^3	18.7 (+10.7)	40.6 (+15.6)	52.7 (+15.2)	84.4 (+7.3)	196.4 (+48.8)	9.8×10^3	24.2 (+9.8)	47.2 (+12.3)	58.3 (+12.5)	89.9 (+5.0)	219.6 (+39.7)
4 × 4	1.6×10^3	16.8 (+8.8)	38.1 (+13.1)	50.0 (+12.5)	83.4 (+6.3)	188.2 (+40.6)	5.6×10^3	21.6 (+7.2)	43.3 (+8.4)	54.3 (+8.5)	88.7 (+3.8)	208.0 (+28.1)

Table 3. Fine-tuning performance for QASIR-L14 and QASIR-L14-336 on the ActivityNet Captions and TVR datasets. Bold and underlined rules are the same as Table 2. Red scores represent the increased points from DL-DKD.

Aggregation	R@1	R@5	R@10	R@100	sumR
Mean	10.1	25.0	35.9	72.2	144.1
Max	7.6	20.0	28.9	63.8	120.2
Query attention	15.7	33.9	50.2	81.4	173.6

Table 4. Zero-shot 2 × 2 QASIR-L14-336 performance when changing the aggregation methods on mean, max, and query attention on the ActivityNet Captions dataset.

	R@1	R@5	R@10	R@100	sumR
Sparse sampling	0.02	0.08	31.0	75.7	106.8
Super images	15.7	33.9	50.2	81.4	173.6

Table 5. A comparison of sparse sampling and 2 × 2 super images. The model and dataset are QASIR-L14-336 and ActivityNet Captions.

datasets.

Is query attention the best? To show the effectiveness of the query-image attention, we report the performance change when replacing the aggregation methods with other global pooling. Table 4 shows that the query attention significantly outperforms other methods, indicating that attending local segments in super images with reference to the input query is essential for PRVR.

Sparse sampling or super images for PRVR? Table 5 shows a comparison of sparse sampling and super images. For a fair comparison, we equalize the computation costs by uniformly sampling $\frac{1}{4}$ frames from 1 × 1 and compare the performance with 2 × 2. The results indicate that super images outperform sparse sampling.

4.2.2 Fine-tuning evaluation

Table 3 shows the fine-tuning performance on the benchmark datasets. Naturally, the fine-tuned models outperform the zero-shot versions and SOTA methods, indicating that our fine-tuning approach is appropriate for large-scale VLMs to boost their performance. In line with the zero-shot experiments, the fine-tuned 1 × 1 achieve the best perfor-

mance with huge computation costs, but 2 × 2 reduces them while maintaining a comparable performance to 1 × 1. In addition, if faster processing is required at the expense of a slight decrease in performance, the fine-tuning approach enables us to increase grid sizes, such as 3 × 3 and 4 × 4. Even with these larger grid sizes, they consistently surpass the SOTA methods.

4.2.3 Moment-to-video performance

As with previous PRVR studies [10, 11], we report grouped sumR based on the moment-to-video ratio (M/V), which is computed as the moment’s length ratio in the entire video duration. The smaller M/V indicates that the videos have less relevant moments with irrelevant content, thereby retrieving them from the corresponding queries is more challenging. As with [11], we compute the sumR scores for three M/V settings, where the moments are short ($r \in (0, 0.2]$), middle ($r \in (0.2, 0.4]$), and long ($r \in (0.4, 1.0]$).

Figure 7 shows M/V results on ActivityNet Captions and TVR, where we reported the scores of SOTA, zero-shot 2 × 2 and 3 × 3 QASIR-L14-336, and their fine-tuned versions. The results demonstrate that the fine-tuned models consistently outperform the SOTA methods in all settings. When comparing QASIR models across different M/V ratios, we observe improved performance as the ratio increases. This suggests that super images excel at retrieving videos containing middle and long moments, rather than short moments. Our future work is to improve the performance in the short moments as much as middle and long moments.

4.2.4 Ablation study

Table 6 shows an ablation study on the fine-tuned QASIR-L14-336. The results indicate that all components contribute to the retrieval performance. When comparing the vision adapter, text adapter, and temporal encoder, two insights emerge. First, the temporal encoder yields the highest performance increase (+20 sumR) among them, but it also incurs the highest increase in computational costs. Second,

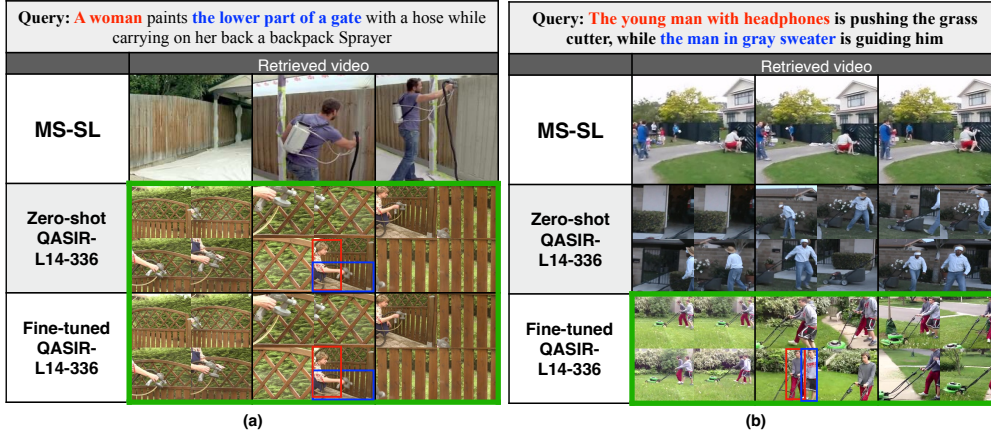


Figure 6. Examples of retrieved videos from different models on the ActivityNet Captions dataset: MS-SL, zero-shot QASIR-L14-336, and its fine-tuned version. The red and blue rectangles represent objects corresponding to the words in the input query. The green frame borders indicate that the videos are successfully retrieved from the input query. Other examples are displayed in the supplementary materials.

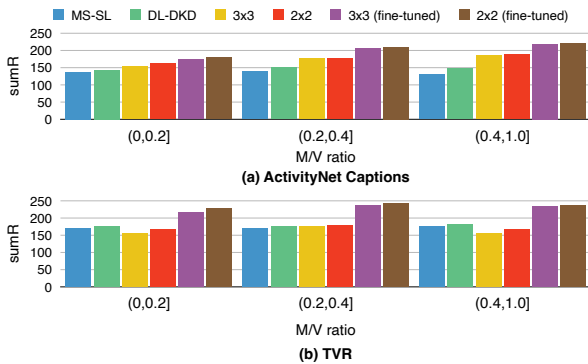


Figure 7. Moment-to-video (M/V) performance on ActivityNet Captions and TVR. 2×2 and 3×3 QASIR-L14-336 are used.

	Δ_{flp}	Δ_{par}	R@1	R@5	R@10	R@100	sumR
Zero-shot	0	0	15.9	34.8	45.8	78.9	175.4
VA	1.1×10^{-4}	0.13	16.0	36.2	48.2	82.8	183.0
TA	7.6×10^{-6}	0.13	18.1	39.6	52.2	85.0	194.9
T	2.2×10^{-3}	3.15	18.4	40.1	52.2	84.7	195.4
VA+TA	1.2×10^{-4}	0.26	19.1	41.2	53.4	84.8	197.6
VA+TA+T	2.3×10^{-3}	3.41	19.3	41.5	53.8	85.3	200.0

Table 6. Ablation study on the fine-tuned 2×2 QASIR-L14-336 on the ActivityNet Captions dataset. VA, TA, T, Δ_{flp} , Δ_{par} represents the vision adapter, text adapter, temporal encoder, and the difference of GFLOPs and parameters (M) from the zero-shot model, respectively.

the text adapter strikes a commendable balance between enhanced performance and computational costs. It achieves comparable performance to the temporal encoder, with only a slight decrease of -0.6 in sumR, while minimizing additional computational costs to a mere 7.6×10^{-6} GFLOPs.

4.2.5 Qualitative results

Figure 6 shows two examples of the retrieved videos from different models: MS-SL, zero-shot QASIR-L14-336, and its fine-tuned version. Although MS-SL correctly recognizes objects in the videos, e.g., “backpack Sprayer” in (a), it misses fine-grained word-level information, such as “A woman,” “the lower part of a gate” in (a) and “young man with headphones” in (b). With a powerful VLM ability, the QASIR-based models can capture such concepts and retrieve videos that match the corresponding query. In addition, by fine-tuning the model, we find that the model acquires a more fine-grained concept to search for correct videos. In (b), the zero-shot QASIR retrieves the video of a man pushing the grass cutter but discards other information. The fine-tuned QASIR can retrieve the correct videos that fully match the corresponding text query.

5. Conclusion

In this study, we proposed an efficient and high-performance PRVR method by combining super images and large-scale VLMs. The super images are created by rearranging the frames onto the $N \times N$ grid layout and can reduce the number of visual encodings to $\frac{1}{N^2}$. This compensates for the low efficiency of large-scale VLMs, allowing us to adopt them as powerful encoders. From our experiments, QASIR achieved promising performance in the zero-shot setting and outperformed SOTA methods using lightweight backbones in the fine-tuning setting while reducing the computation costs. In addition, we obtained insights by varying model settings for optimal balance between the retrieval performance and computation costs.

TV show title	#Videos	TVR				sumR
		R@1	R@5	R@10	R@100	
The Big Bang Theory	2,155	22.6	42.6	53.1	84.4	202.7
How I Met Your Mother	745	24.8	43.4	54.6	87.2	210.1
Friends	2,800	19.5	36.8	46.4	81.0	183.8
Grey’s Anatomy	520	15.9	32.1	40.2	78.1	166.3
House	2,310	11.9	24.3	31.6	66.0	133.9
Castle	2,365	12.4	26.6	33.8	68.7	141.5
Total	10,835	17.2	33.3	42.1	76.1	168.7

Table 7. Zero-shot retrieval performance on each TV show. We use the 2×2 QASIR-L14-336 as our base model.

noun gap. To demonstrate this, we show word clouds¹ generated from query sentences in the test set on each dataset (Figure 9). As the word clouds suggest, general objects, such as “man,” and “woman,” appear frequently in the ActivityNet Captions [22], while the character names, such as “Beckett,” “Leonard,” and “Sheldon” appear frequently in TVR [23]. Therefore, if VLMs do not know the link between these names and their visual representations, they cannot retrieve the corresponding videos from input queries successfully. This is the reason for decreased zero-shot performance in TVR and increased fine-tuning performance by enabling models to understand their linking and outperform previous SOTA methods.

Performance across TV shows. Then, a question arises, *How much do VLMs know the TV shows that TVR covers?* If VLMs do not see them completely, VLMs perform poorly because of disjoint between characters and their visual representations. To investigate them, we aggregate the zero-shot performance on each TV show. Table 7 shows the result, presenting a large performance gap across TV shows. There is a 76.2 sumR gap between the highest (How I Met Your Mother) and lowest (House). Therefore, we infer that VLMs possess knowledge of these TV shows to some extent, but their understanding is influenced by biases that stem from their training dataset. Because the VLM backbone is OpenAI CLIP-L/14-336 [33] pre-trained on private data, further analysis of the training data to determine its inclusion of images from these TV shows is infeasible.

C.2. Performance change w.r.t. query length

The queries in the benchmark datasets have different lengths. We assume that the query length S affects the retrieval performance because shorter ones are less informative than the longer ones to distinguish videos. To verify this, we investigate the sumR aggregated on query length for three groups, short ($S \leq 10$), medium ($10 < S \leq 15$), and long ($15 < S$). Figure 10 presents the performance change w.r.t query length. As we expected, all of the models decrease their performance on short queries, rather than longer queries. To address this issue, one of the promising

¹To generate word clouds, we use this library: https://amueller.github.io/word_cloud/

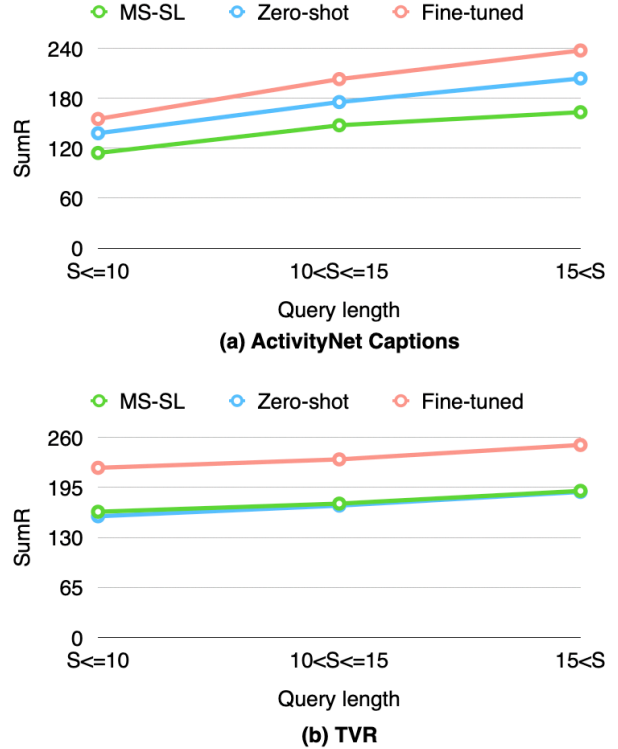


Figure 10. Performance aggregated on query length for three groups, short ($S \leq 10$), medium ($10 < S \leq 15$), and long ($S > 15$), where S represents query length, the number of words in the query.

ideas is to enhance queries from human feedback. Interactive video retrieval was recently introduced [26], which asks questions to humans to retrieve videos accurately. We think that it is an interesting future direction to incorporate our idea of combining super images and large-scale VLMs into interactive video retrieval.

C.3. Retrieval examples

Figure 11 shows additional retrieval examples. (a) and (b) are successful cases in TVR. Because we display two ActivityNet Captions examples in the main paper, we display two TVR examples in this supplementary material. (c) and (d) are failure cases of QASIR. Here, we first discuss the successful cases in TVR, then discuss failure cases and the limitations of our approach.

Successful cases in TVR. As described in Section C.1, if the VLMs know the linking between characters and their visual representations, the zero-shot model can retrieve videos correctly. (a) belongs to The Big Bang Theory, and as shown in Table 7, the zero-shot model knows it and achieves strong retrieval performance. Therefore, in (a), it correctly recognizes Sheldon and Leonard and understands their relationship with Sheldon using a fake steering wheel and

Successful cases in TVR

Query: Sheldon uses a fake steering wheel connected to a computer while Leonard stands behind him		Query: Erica sits at a the table and grabs her pregnant stomach in pain while talking to Monica, Phoebe, Chandler and Joey	
		Retrieved video	
MS-SL		MS-SL	
Zero-shot QASIR-L14-336		Zero-shot QASIR-L14-336	
Fine-tuned QASIR-L14-336		Fine-tuned QASIR-L14-336	

(a) (b)

QASIR failure cases

Query: A woman is seated on a work table and holds a paint brush		Query: Brennan grabs Stark and lifts him up off of the bed	
		Retrieved video	
MS-SL		MS-SL	
Zero-shot QASIR-L14-336		Zero-shot QASIR-L14-336	
Fine-tuned QASIR-L14-336		Fine-tuned QASIR-L14-336	

(c): $M/V = 0.07$, ActivityNet (d): $M/V = 0.09$, TVR

Figure 11. Additional examples of retrieved videos from different models. We provide two successful cases (a) and (b), and two failure cases (c) and (d). red, blue, and magenta rectangles represent objects corresponding to the words in the input query. The green frame borders indicate that the videos are successfully retrieved from the input query.

Leonard standing behind him. MS-SL [10] fails to capture this relationship, retrieving a video that Sheldon is standing

behind Leonard. The fine-tuning enables the model to understand videos that the zero-shot models cannot capture.

For example, in (b), the zero-shot model recognizes a pregnant woman but the character is not Erica. The fine-tuned version can recognize Erica correctly and understand the situation, where Erica is pregnant and sitting at the table.

Failure cases and limitations. Although the fine-tuned model achieves higher retrieval performance than MS-SL, it sometimes fails to retrieve videos. As described in moment-to-video (M/V) retrieval performance in Section 4.2.3 in the main paper, our approach tends to miss shorter ($r < 0.2$) moments. The M/V ratios of (c) and (d) are 0.07 and 0.09. Owing to dense frame representations, MS-SL can capture such very short moments correctly but our approach misses them. In addition to the temporal encoder in Section 3.3 in the main paper, spatial attention on grids may be one of the approaches to this problem, which is our future work.

References

- [1] Dzmitry Bahdanau, Kyunghyun Cho, and Yoshua Bengio. Neural machine translation by jointly learning to align and translate. In *International Conference on Learning Representations*, 2015. 4
- [2] Max Bain, Arsha Nagrani, Gül Varol, and Andrew Zisserman. Frozen in time: A joint video and image encoder for end-to-end retrieval. In *Proceedings of the IEEE/CVF International Conference on Computer Vision*, pages 1728–1738, 2021. 2
- [3] Max Bain, Arsha Nagrani, Gül Varol, and Andrew Zisserman. A clip-hitchhiker’s guide to long video retrieval. *arXiv preprint arXiv:2205.08508*, 2022. 2
- [4] Peijun Bao, Qian Zheng, and Yadong Mu. Dense events grounding in video. In *Proceedings of the AAAI Conference on Artificial Intelligence*, pages 920–928, 2021. 1, 2
- [5] Hakan Bilen, Basura Fernando, Efstratios Gavves, Andrea Vedaldi, and Stephen Gould. Dynamic image networks for action recognition. In *Proceedings of the IEEE Conference on Computer Vision and Pattern Recognition*, pages 3034–3042, 2016. 3
- [6] Shizhe Chen, Yida Zhao, Qin Jin, and Qi Wu. Fine-grained video-text retrieval with hierarchical graph reasoning. In *Proceedings of the IEEE/CVF Conference on Computer Vision and Pattern Recognition*, pages 10638–10647, 2020. 1, 2
- [7] James Davis and Aaron Bobick. The representation and recognition of action using temporal templates. In *Proceedings of the IEEE International Conference on Computer Vision*, pages 2736–2744, 1997. 3
- [8] Jianfeng Dong, Xirong Li, and Cees GM Snoek. Predicting visual features from text for image and video caption retrieval. *IEEE Transactions on Multimedia*, 20(12):3377–3388, 2018. 1, 2
- [9] Jianfeng Dong, Xirong Li, Chaoxi Xu, Xun Yang, Gang Yang, Xun Wang, and Meng Wang. Dual encoding for video retrieval by text. *IEEE Transactions on Pattern Analysis and Machine Intelligence*, 2021. 2
- [10] Jianfeng Dong, Xianke Chen, Minsong Zhang, Xun Yang, Shujie Chen, Xirong Li, and Xun Wang. Partially relevant video retrieval. In *Proceedings of the 29th ACM International Conference on Multimedia*, pages 246–257, 2022. 1, 2, 5, 6, 7, 9, 11
- [11] Jianfeng Dong, Minsong Zhang, Zheng Zhang, Xianke Chen, Daizong Liu, Xiaoye Qu, Xun Wang, and Baolong Liu. Dual learning with dynamic knowledge distillation for partially relevant video retrieval. In *Proceedings of the IEEE/CVF International Conference on Computer Vision*, pages 11302–11312, 2023. 1, 2, 5, 6, 7, 9
- [12] Quanfu Fan, Chun-Fu Chen, and Rameswar Panda. Can an image classifier suffice for action recognition? In *International Conference on Learning Representations*, 2022. 2, 3
- [13] Yuxin Fang, Quan Sun, Xinggang Wang, Tiejun Huang, Xinlong Wang, and Yue Cao. Eva-02: A visual representation for neon genesis. *arXiv preprint arXiv:2303.11331*, 2023. 6
- [14] Yuxin Fang, Wen Wang, Binhui Xie, Quan Sun, Ledell Wu, Xinggang Wang, Tiejun Huang, Xinlong Wang, and Yue Cao. Eva: Exploring the limits of masked visual representation learning at scale. In *Proceedings of the IEEE/CVF Conference on Computer Vision and Pattern Recognition*, pages 19358–19369, 2023. 2
- [15] Peng Gao, Shijie Geng, Renrui Zhang, Teli Ma, Rongyao Fang, Yongfeng Zhang, Hongsheng Li, and Yu Qiao. Clip-adapter: Better vision-language models with feature adapters. *International Journal of Computer Vision*, 2023. 4, 5, 9
- [16] Ning Han, Jingjing Chen, Guangyi Xiao, Hao Zhang, Yawen Zeng, and Hao Chen. Fine-grained cross-modal alignment network for text-video retrieval. In *Proceedings of the 29th ACM International Conference on Multimedia*, pages 3826–3834, 2021. 1, 2
- [17] Kaiming He, Xiangyu Zhang, Shaoqing Ren, and Jian Sun. Deep residual learning for image recognition. In *Proceedings of the IEEE Conference on Computer Vision and Pattern Recognition*, pages 770–778, 2016. 2
- [18] Neil Houlsby, Andrei Giurgiu, Stanislaw Jastrzebski, Bruna Morrone, Quentin De Laroussilhe, Andrea Gesmundo, Mona Attariyan, and Sylvain Gelly. Parameter-efficient transfer learning for NLP. In *Proceedings of the 36th International Conference on Machine Learning*, pages 2790–2799, 2019. 4
- [19] Fan Hu, Aozhu Chen, Ziyue Wang, Fangming Zhou, Jianfeng Dong, and Xirong Li. Lightweight attentional feature fusion: A new baseline for text-to-video retrieval. In *Proceedings of the 17th European Conference on Computer Vision*, 2022. 1, 2
- [20] Shaohan Huang, Li Dong, Wenhui Wang, Yaru Hao, Saksham Singhal, Shuming Ma, Tengchao Lv, Lei Cui, Owais Khan Mohammed, Barun Patra, Qiang Liu, Kriti Aggarwal, Zewen Chi, Johan Bjorck, Vishrav Chaudhary, Subhojit Som, Xia Song, and Furu Wei. Language is not all you need: Aligning perception with language models. In *Advances in Neural Information Processing Systems*, 2023. 2
- [21] Jared Kaplan, Sam McCandlish, Tom Henighan, Tom B. Brown, Benjamin Chess, Rewon Child, Scott Gray, Alec Radford, Jeffrey Wu, and Dario Amodei. Scaling laws for

- neural language models. *arXiv preprint arXiv:2001.08361*, 2020. [2](#)
- [22] Ranjay Krishna, Kenji Hata, Frederic Ren, Li Fei-Fei, and Juan Carlos Niebles. Dense-captioning events in videos. In *Proceedings of the IEEE/CVF International Conference on Computer Vision*, pages 706–715, 2017. [1](#), [2](#), [5](#), [10](#)
- [23] Jie Lei, Licheng Yu, Tamara L Berg, and Mohit Bansal. TVR: A large-scale dataset for video-subtitle moment retrieval. In *European Conference on Computer Vision*, pages 447–463, 2020. [2](#), [5](#), [10](#)
- [24] Jie Lei, Linjie Li, Luowei Zhou, Zhe Gan, Tamara L. Berg, Mohit Bansal, and Jingjing Liu. Less is more: Clipbert for video-and-language learning via sparse sampling. In *Proceedings of the IEEE/CVF Conference on Computer Vision and Pattern Recognition*, pages 7331–7341, 2021. [2](#)
- [25] Jie Lei, Tamara Berg, and Mohit Bansal. Revealing single frame bias for video-and-language learning. In *Proceedings of the 61st Annual Meeting of the Association for Computational Linguistics*, pages 487–507, 2023. [2](#)
- [26] Kaiqu Liang and Samuel Albanie. Simple baselines for interactive video retrieval with questions and answers. In *Proceedings of the IEEE/CVF International Conference on Computer Vision*, pages 11091–11101, 2023. [10](#)
- [27] Hongying Liu, Ruyi Luo, Fanhua Shang, Mantang Niu, and Yuan Yuan Liu. Progressive semantic matching for video-text retrieval. In *Proceedings of the 29th ACM International Conference on Multimedia*, pages 5083–5091, 2021. [1](#), [2](#)
- [28] Yinhan Liu, Myle Ott, Naman Goyal, Jingfei Du, Mandar Joshi, Danqi Chen, Omer Levy, Mike Lewis, Luke Zettlemoyer, and Veselin Stoyanov. RoBERTa: A robustly optimized bert pretraining approach. *arXiv preprint arXiv:1907.11692*, 2019. [5](#)
- [29] Ze Liu, Yutong Lin, Yue Cao, Han Hu, Yixuan Wei, Zheng Zhang, Stephen Lin, and Baining Guo. Swin transformer: Hierarchical vision transformer using shifted windows. In *Proceedings of the IEEE/CVF International Conference on Computer Vision*, pages 10012–10022, 2021. [3](#)
- [30] Ilya Loshchilov and Frank Hutter. Decoupled weight decay regularization. In *International Conference on Learning Representations*, 2019. [5](#)
- [31] Antoine Miech, Jean-Baptiste Alayrac, Lucas Smaira, Ivan Laptev, Josef Sivic, and Andrew Zisserman. End-to-end learning of visual representations from uncurated instructional videos. In *Proceedings of the IEEE/CVF Conference on Computer Vision and Pattern Recognition*, pages 9879–9889, 2020. [2](#)
- [32] Zhaofan Qiu, Ting Yao, Yan Shu, Chong-Wah Ngo, and Tao Mei. Condensing a sequence to one informative frame for video recognition. In *Proceedings of the IEEE/CVF International Conference on Computer Vision*, pages 16311–16320, 2021. [3](#)
- [33] Alec Radford, Jong Wook Kim, Chris Hallacy, Aditya Ramesh, Gabriel Goh, Sandhini Agarwal, Girish Sastry, Amanda Askell, Pamela Mishkin, Jack Clark, Gretchen Krueger, and Ilya Sutskever. Learning transferable visual models from natural language supervision. In *Proceedings of the 38th International Conference on Machine Learning*, pages 8748–8763, 2021. [2](#), [4](#), [10](#)
- [34] Aleksandar Shtedritski, Christian Rupprecht, and Andrea Vedaldi. What does clip know about a red circle? visual prompt engineering for vlms. In *Proceedings of the IEEE/CVF International Conference on Computer Vision*, pages 11987–11997, 2023. [2](#)
- [35] Yale Song and Mohammad Soleymani. Polysemous visual-semantic embedding for cross-modal retrieval. In *Proceedings of the IEEE/CVF Conference on Computer Vision and Pattern Recognition*, pages 1979–1988, 2019. [1](#), [2](#)
- [36] Mohammad Tavakolian, Mohammad Sabokrou, and Abdenour Hadid. Avd: Adversarial video distillation. *arXiv preprint arXiv:1907.05640*, 2019. [3](#)
- [37] Mohammad Tavakolian, Hamed R. Tavakoli, and Abdenour Hadid. Awsd: Adaptive weighted spatiotemporal distillation for video representation. In *Proceedings of the IEEE/CVF International Conference on Computer Vision*, pages 8020–8029, 2019. [3](#)
- [38] Ashish Vaswani, Noam Shazeer, Niki Parmar, Jakob Uszkoreit, Llion Jones, Aidan N. Gomez, Lukasz Kaiser, and Illia Polosukhin. Attention is all you need. In *Advances in Neural Information Processing Systems*, pages 5998–6008, 2017. [4](#)
- [39] Jinpeng Wang, Yixiao Ge, Rui Yan, Yuying Ge, Kevin Qinghong Lin, Satoshi Tsutsui, Xudong Lin, Guanyu Cai, Jianping Wu, Ying Shan, Xiaohu Qie, and Mike Zheng Shou. All in one: Exploring unified video-language pre-training. In *Proceedings of the IEEE/CVF Conference on Computer Vision and Pattern Recognition*, pages 6598–6608, 2023. [2](#)
- [40] Wei Wang, Junyu Gao, Xiaoshan Yang, and Changsheng Xu. Learning coarse-to-fine graph neural networks for video-text retrieval. *IEEE Transactions on Multimedia*, 2020. [1](#), [2](#)
- [41] Chao-Yuan Wu and Philipp Krahenbuhl. Towards long-form video understanding. In *Proceedings of the IEEE/CVF Conference on Computer Vision and Pattern Recognition*, pages 1884–1894, 2021. [4](#)
- [42] Yang Wu, Shilong Wang, Hao Yang, Tian Zheng, Hongbo Zhang, Yanyan Zhao, and Bing Qin. An early evaluation of gpt-4v(ision). *arXiv preprint arXiv:2310.16534*, 2023. [2](#)
- [43] Hu Xu, Gargi Ghosh, Po-Yao Huang, Dmytro Okhonko, Armen Aghajanyan, Florian Metze, Luke Zettlemoyer, and Christoph Feichtenhofer. VideoCLIP: Contrastive pre-training for zero-shot video-text understanding. In *Proceedings of the Conference on Empirical Methods in Natural Language Processing*, pages 6787–6800, 2021. [2](#)
- [44] Yuting Xu, Jian Liang, Gengyun Jia, Ziming Yang, Yanhao Zhang, and Ran He. TALL: Thumbnail layout for deepfake video detection. In *Proceedings of the IEEE/CVF International Conference on Computer Vision*, pages 22658–22668, 2023. [2](#), [3](#)
- [45] Gengyuan Zhang, Jisen Ren, Jindong Gu, and Volker Tresp. Multi-event video-text retrieval. In *Proceedings of the IEEE/CVF International Conference on Computer Vision*, pages 22113–22123, 2023. [1](#), [2](#)
- [46] Luowei Zhou, Chenliang Xu, and Jason J. Corso. Towards automatic learning of procedures from web instructional videos. In *Proceedings of the AAAI Conference on Artificial Intelligence*, pages 7590–7598, 2018. [1](#), [2](#)